The Tropical Convective Evolution in Different Rain Types over the West and East Pacific

Yi-Chien Chen[1] and Hirohiko Masunaga[2]

[1]*Graduate School of Environmental Studies, Nagoya University, Nagoya, Japan*
[2]*Institute for Space-Earth Environmental Research, Nagoya University, Nagoya, Japan*

(Manuscript received 22 August 2024, accepted 22 October 2024)

Abstract The TRMM PR and GSMaP products are analyzed to examine the variability in different types of precipitation under three rain intensity classes for investigating the evolution of tropical convection over the tropical western Pacific (WP) and eastern Pacific (EP). Composite time series are constructed around the GSMaP precipitation maxima for different precipitation types identified from the TRMM PR. The composite evolution is further broken down into weak, moderate, and strong rains, divided by applying quartile-based thresholds to rainfall maxima. The results show that the evolution of deep convection reaches a precipitation peak earlier by a few hours than stratiform evolution precipitation for strong and moderate rain regardless of the region. Deep convective rain still predominates in the WP weak rain, while shallow precipitation dominates the weak rain in EP. The composite time series of vertical velocity is overall physically consistent with the expectation from these findings. It is implied that the convective-stratiform lag and tilted updraft structure for strong rain are shared between WP and EP, while the attribution of weak rain can differ significantly between the regions.

Citation: Chen, Y.-C., and H. Masunaga, 2024: The tropical convective evolution in different rain types over the West and East Pacific. *SOLA*, **20**, 392−399, doi:10.2151/sola.2024-052.

1. Introduction

The vertical motion profiles in the western Pacific (WP) region climatologically exhibit a top-heavy structure, whereas the vertical motion profiles display a bottom-heavy pattern in the eastern Pacific (EP) region (Trenberth et al. 2000; Zhang et al. 2004; Back and Bretherton 2006). The top-heaviness of vertical motion shapes the vertical structure of horizontal convergence through mass conservation, which is in turn closely related to precipitation so it is nearly balanced with the moisture convergence. The regional contrast between the top-heavy and bottom-heavy vertical velocity profiles is hence tightly coupled with the geographical pattern of tropical moist convection.

Past analyses of radiosonde data have shown that the relatively warm and moist air at a low level in WP increases the relative humidity in the mid and upper troposphere through deep convection in the top-heavy structure of vertical motion (Numaguti et al. 1995; Ushiyama et al. 1995; Yoneyama and Fujitani 1995; Johnson and Lin 1997; Sherwood 1999; Sobel et al. 2004). Simple models explain that low-level convergence is driven by a strong Sea Surface Temperature (SST) gradient, influencing the regional dependence of vertical motion profiles (Lindzen and Nigam 1987; Back and Bretherton 2009). Although total rainfall is comparable in magnitude between WP and EP, surface convergence in EP is approximately twice as large as that in WP (Back and Bretherton 2009b; Yokoyama and Takayabu 2012; Handlos and Back 2014). As such, the physical processes connecting precipitation and the large-scale dynamics associated with it vary from one region to another across the tropics.

On the other hand, tropical organized convective systems, initiated typically with a gradually deepening of convection induced by low-level heating, eventually develop into deep convective and stratiform clouds, commonly seen across a hierarchy of different scales including convectively coupled equatorial waves, MJO, and mesoscale convective systems (MCS) (Takayabu et al. 1996; Benedict and Randall 2007; Mapes et al. 2006; Kiladis et al. 2009; Lappen and Schumacher 2012, 2014; Inoue and Back 2015). This structure can be broadly categorized into three stages: shallow precipitation in the initial phase, deep convective precipitation in the intensifying phase, and stratiform precipitation from the mature to decaying phases (Houze 1989, 1997; Johnson et al. 1999; Mapes et al. 2006; Zhang and Klein 2010; Lamer et al. 2015; Powell 2016; Kurowski et al. 2018; Vogel et al. 2020; Schumacher and Houze 2003). Such a spectrum of cloud structures may account for the diabatic heating profiles, which are regionally variable in climatological characteristics across the tropics (Frank and McBride 1989; Schumacher et al. 2004). Recent research also suggests that the vertical profile structure is not uniquely related to the stratiform and shallow rain fraction (Back et al. 2017; Shige et al. 2007).

While the regional gradient in the characteristics of tropical convection is well known, it remains unclear how they

Corresponding author: Yi-Chien Chen, Graduate School of Environmental Studies, Nagoya University, Nagoya, Japan. E-mail: chen.yi-chien.u6@s.mail.nagoya-u.ac.jp.

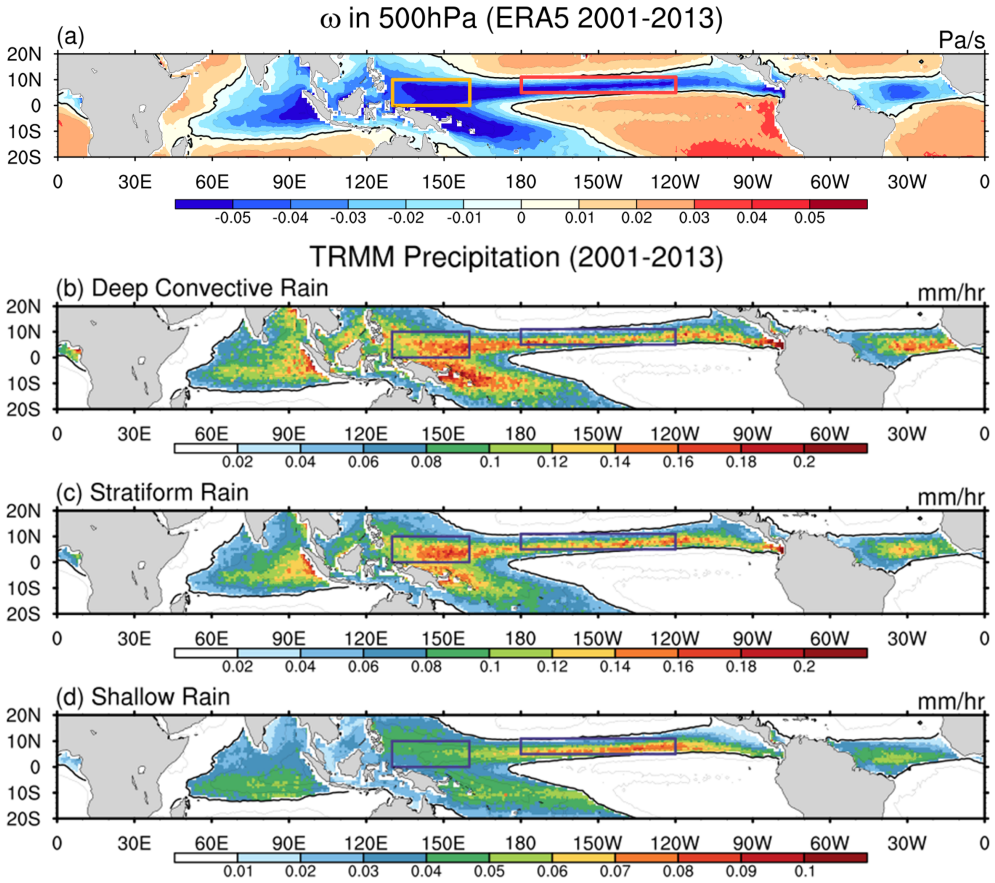

Fig. 1. The spatial distribution of climatological (a) vertical pressure velocity at 500 hPa ($\bar{\omega}_{500}$), (b) deep convective precipitation, (b) stratiform precipitation, and (d) shallow precipitation over the period from 2001–2013. The black curves showed the boundary of the ITCZ region, where the climatological vertical pressure velocity at 500 hPa is zero. The rectangular boxes mark the two target regions for analyzing the regional differences in precipitation composition, which include the western Pacific (WP) (0°–10°N/130°E–160°E; yellow) and eastern Pacific (EP) (5°N–11°N/180°–120°E; red).

vary over time during the lifecycle of convective systems. A major challenge is that TRMM PR and Global Precipitation Measurement (GPM) Dual-frequency Precipitation Radar (DPR), optimal instruments to differentiate the different rain types (shallow, deep convective, and stratiform), are difficult to put into the context of convective lifecycle because their low-Earth orbits do not allow temporally continuous observations. In this study, an analysis strategy is devised to overcome this limitation by combining TRMM PR measurements with a high-resolution global precipitation data product. This study aims to explore the fundamental properties, vertical structure, and regional differences of convective clouds (deep convective, stratiform, and shallow precipitation) by using continuous composite time series based primarily on satellite observations. The composite time series will be further decomposed into different rainfall intensity classes (strong rain, moderate rain, and weak rain) to examine the composition of precipitation in various regions, providing new insights into the regional variations in the convective lifecycle.

2. Data

A combination of reanalysis data and satellite observation data is utilized in this study to examine the precipitating cloud properties and the vertical velocity structure over the regional differences in the tropics. The atmospheric reanalysis dataset used in this work is the European Centre for Medium-Range Weather Forecasts (ECMWF) ERA5 product (Hersbach et al. 2020). This work adopts the ERA5 vertical velocity (ω) to supplement satellite data, from which vertical velocity is unavailable. We analyze the hourly ERA5 data re-gridded horizontally to a 1° × 1° grid. The blue-colored area over tropical oceans in Figure 1a is hereafter referred to as the Intertropical Convergence Zone (ITCZ), which is the region where the climatological vertical pressure velocity at 500 hPa is less than or equal to 0 ($\bar{\omega}_{500} \leq 0$). The yellow and red boxes in Fig. 1a show the location of the target domain of WP (0°–10°N/130°E–160°E) and EP (5°N–11°N/180°E–120°E) to be analyzed in this work.

Corresponding to the temporal and spatial intervals of the ERA5 reanalysis data, the Tropical Rainfall Measuring Mission (TRMM) Precipitation Radar (PR) version 07 (equivalent to version 9 in the now-obsolete nomenclature)

Table 1. The definition and the calculation from TRMM of each precipitation type in this study.

Precipitation Types	TRMM PR rain-type	Additional Condition
Deep Convective	Convective	stormTopHeight ≥ meltLevel
Stratiform	Stratiform	/
Shallow	Convective	stormTopHeight < meltLevel

for the 13-year period from 2001 to 2013 and re-gridded to 1° × 1° grid is adopted for precipitation. The near-surface precipitation is classified into deep convective precipitation, stratiform precipitation, and shallow precipitation based on the TRMM PR rain-type flag with an additional constraint on storm-top height (stormTopHeight) in this study. The deep convective and shallow cumulus types belong to the convective type but are separated by whether stormTopHeight is higher or lower than the melting level (meltLevel) (see Table 1). Figures 1b–d show the spatial distribution of deep convective, stratiform, and shallow precipitation under this classified definition.

Regarding the selection of precipitation data, although GPM DPR has the advantage over TRMM PR in that DPR is more sensitive to light rain than PR. On the other hand, TRMM has its own advantages over the GPM core observatory. First, the TRMM orbit has a lower inclination angle than the GPM, allowing denser observations at tropical latitudes. Second, the repeat cycle in diurnal sampling is shorter for TRMM (46 days) than for GPM (83 days), so that diurnal sampling is more quickly homogenized. Finally, the GPM period contains an exceptionally strong El Niño event from 2014 to 2016, which could be highly unrepresentative of the climatological regional contrast between WP and EP. For these reasons, the TRMM data record from 2001 to 2013 has been chosen for this analysis.

Global Satellite Mapping of Precipitation (GSMaP) is used for complementing the TRMM data. In this study, GSMaP Gauge RNL version 6 (Kubota et al. 2020) is utilized for identifying the local temporal maxima of surface rain to define composite time series as described later, taking advantage of the temporally and spatially continuous coverage of GSMaP, unlike sporadic TRMM satellite overpasses.

3. Methodology

3.1 Composite time series

The evolution of convective systems over their lifecycle is analyzed with the composite time series of surface precipitation and ω in this study. Masunaga (2012, 2013, 2014) explored an analysis method to combine measurements from multiple satellites in different orbits into a statistically continuous time series. In this study, we develop a similar strategy using the local maxima in GSMaP rainfall as the foundation of the composite time series calculation. A 5-hour running mean is applied to the GSMaP rainfall and TRMM PR precipitation before calculating the composite time series, ensuring that the data is not affected by undesirable noisy fluctuations. Whenever GSMaP rainfall is found to reach a local temporal peak, the timing of the precipitation peak defines the base point in the composite time series. A sequence of TRMM and ERA5 variables that fall within ±72 h about the precipitation peak (0 h) is then collected as samples that are eventually composited into a 144-hour-long time series. Repeating this procedure to all GSMaP precipitation peaks for all grid points in each study domain, one obtains a large size of samples having different leads or lags from the precipitation peak. Although individual TRMM observations are sporadic on an instantaneous basis, the composite time series constructed this way allows to study statistically continuous temporal variability as the collected samples are averaged together in each hourly bin. The same composite was tested with Integrated Multi-satellite Retrievals for GPM (IMERG) (Huffman et al. 2019) instead of GSMaP (Fig. S1). The result is insensitive to the datasets in use.

3.2 Rainfall intensity classes

The composite time series is broken down into three rainfall intensity classes: strong, moderate, and weak rain. The definition of these classes is based on quartiles in the Cumulative Probability Function (CPF) of precipitation. The CPF is calculated with the 13-year GSMaP precipitation over the whole ITCZ ($\overline{\omega}_{500} \leq 0$), binned into every 0.01 mm hr^{-1} exclusive of zero precipitation. The first (25%), second (50%), and third quartiles (75%) are found to be 0.08 mm hr^{-1}, 0.45 mm hr^{-1}, and 1.67 mm hr^{-1}, respectively. The weak-rain category is defined when the GSMaP precipitation peak is lower than 0.45 mm hr^{-1}, moderate rain for precipitation peaks between 0.45 mm hr^{-1} and 1.67 mm hr^{-1}, and strong rain for precipitation peaks greater than or equal to 1.67 mm hr^{-1}. The composite time series is separated by applying these thresholds so the evolution of convective systems is sorted by different rainfall intensities. Table 2 shows the sample numbers of the composite statistics.

Figure 2 shows the composite time series of total precipitation in different rainfall intensity classes and regions. Strong and moderate rains appear almost identical across various regions for total precipitation. In contrast, the regional

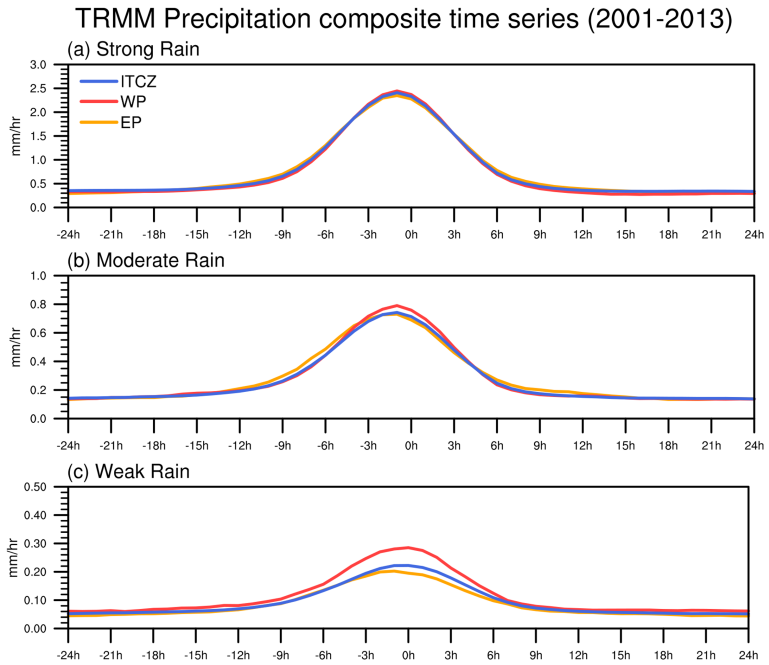

Fig. 2. The composite time series of total precipitation in (a) strong rain, (b) moderate rain, and (c) weak rain among ITCZ (blue line), WP (red line), and EP (yellow line) within the time period from −24 h to 24 h.

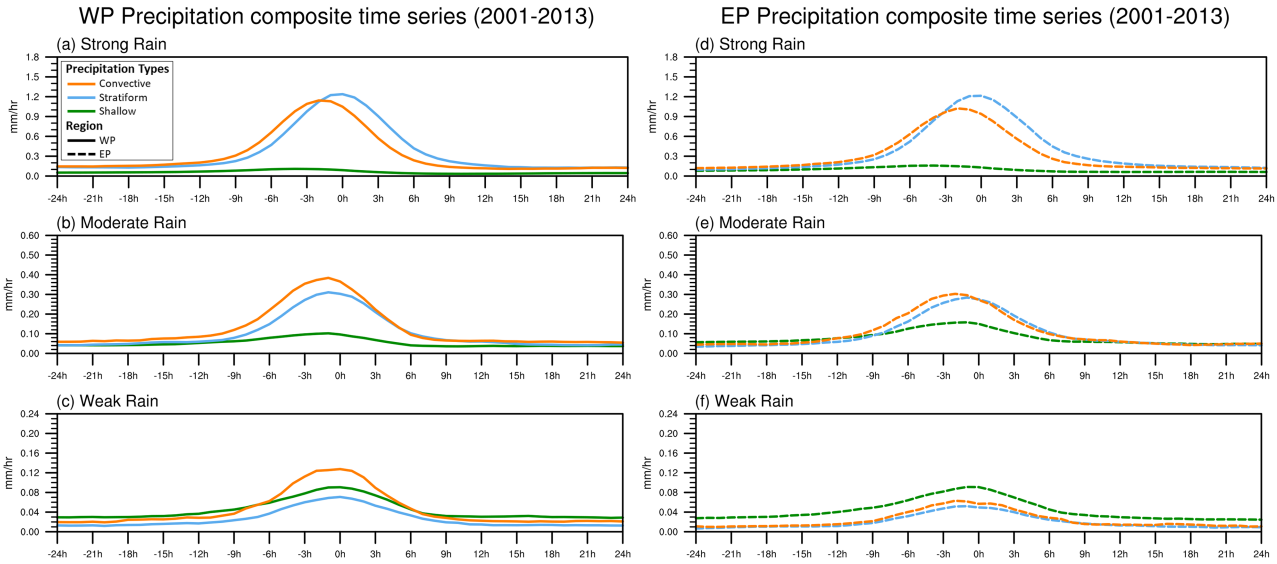

Fig. 3. The composite time series of deep convective precipitation (orange line), stratiform precipitation (blue line), and shallow precipitation (green line) within the time period from −24 h to 24 h in (a), (d) strong rain, (b), (e) moderate rain, and (c), (f) weak rain in the western Pacific (solid) and the eastern Pacific (dashed), respectively.

differences seem obvious for weak rain. During the convectively active period (roughly within ±6 h), the intensity of weak rain in the WP is higher than in the ITCZ and EP, with EP being the weakest among the three. This suggests that the mechanism of convective evolution may have a notable regional dependence for weak rain while much less for strong and moderate rains. More details will be discussed in the result section below.

4. Results

The total precipitation in Fig. 2 above is decomposed into deep convective, stratiform, and shallow rain, separately for WP and EP in Fig. 3. The peak hours of deep convective and stratiform curves slightly deviated against each other for strong rain (Figs. 3a and 3d), but the peak-hour difference becomes less noticeable for moderate and weak rains. The peak of strong rain occurs earlier for deep convection by a few hours than for stratiform rain, aligning with the existing knowledge of the MCS lifecycle. Moderate rain (Figs. 3b and 3e) has essentially the same evolutionary characteristics

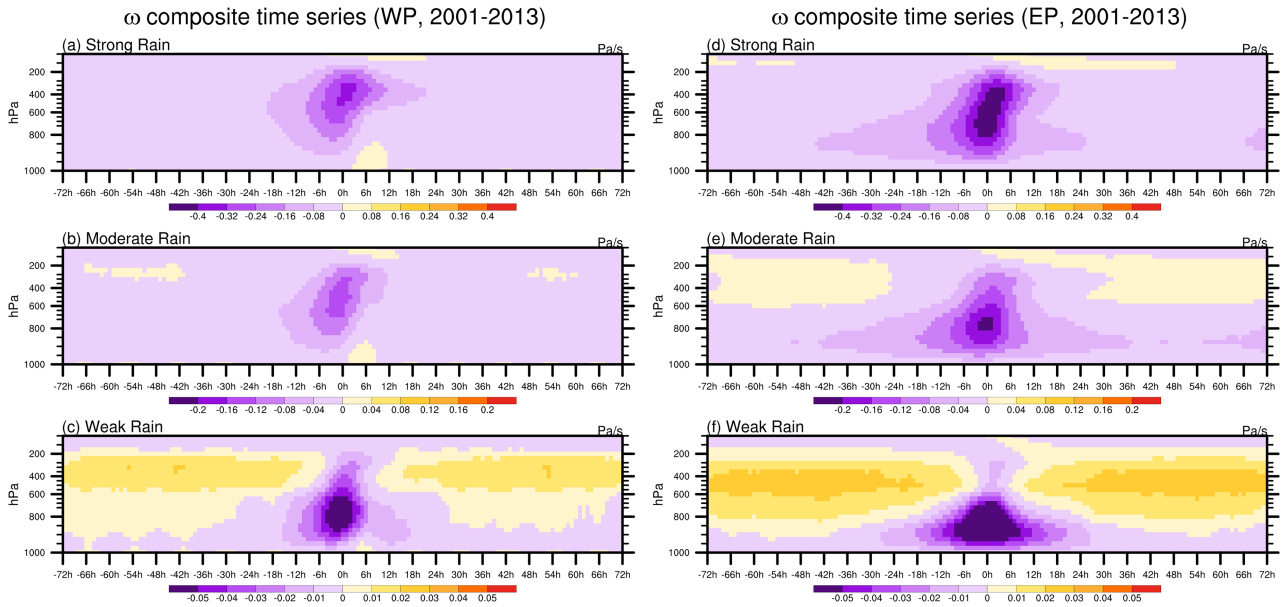

Fig. 4. The composite time series of omega in (a) strong rain, (b) moderate rain, and (c) weak rain in the western Pacific and (d) strong rain, (e) moderate rain, and (f) weak rain in the eastern Pacific.

as heavy rain in WP. The moderate rain in EP consists of a qualitatively similar variability of deep convective and stratiform rain but with a somewhat suppressed amplitude compared to the WP counterpart.

At the same time, moderate rain in EP exhibits a higher contribution of shallow precipitation than in WP, although the total rainfall did not imply any visible regionality in Fig. 2. Weak rain (Figs. 3c and 3f) is very contrasting between the regions. In WP, deep convective precipitation still predominates in weak rain, whereas shallow precipitation dominates weak rain in EP. The weak rain over WP is brought about primarily by deep convection that, unlike the strong and moderate rains, does not accompany significant stratiform precipitation and hence is likely to be isolated convection rather than organized systems. On the other hand, the driver of the EP weak rain is mainly shallow convection with little contribution of deep convective or stratiform precipitation. Shallow convection, by construction unable to develop beyond the freezing level, lacks any mechanism to drive top-heavy ascent. It follows that while the characteristics of organized systems are overall shared between WP and EP for strong and moderate rain, the mechanisms of weak rain formation differ entirely between the regions.

The peak of TRMM precipitation in Figs. 2 and 3 occurs approximately 1–2 hours earlier than the peak of GSMaP. TRMM primarily relies on microwave observations, while GSMaP combines microwave and infrared measurements. The inclusion of infrared brightness temperature likely detects extensive stratiform anvils more preferentially than spatially confined convective cores. This presumably explains why the GSMaP precipitation peak coincides with the stratiform peak, as seen in Figs. 3a and 3d. The convective and shallow peaks come slightly earlier, because these rain types occur before the stratiform rain develops in the typical convective lifecycle.

These regional differences in precipitation are echoed to a certain degree by the vertical velocity structure. Figure 4 displays the composite time series of vertical velocity for different rainfall intensity classes in WP and EP. It is well-known that WP climatologically exhibits a top-heavy structure, while a bottom-heavy structure is typical of EP. From the composite time series for strong and moderate rain (Figs. 4a, 4b, 4d, and 4e), it is evident that the tilted characteristics of the MSC lifecycle are present during the convectively active period. This corresponds well to the development of deep convection to stratiform precipitation structures as indicated in Fig. 3. EP is more bottom-heavy in the peak-hour vertical velocity than WP particularly for moderate rain, consistent with the expectation from an enhanced relative contribution of shallow precipitation in EP as implied by Fig. 3e. Figures 4c and 4f show the vertical velocity structure in weak rain for WP and EP. EP exhibits a robust upward motion confined strictly to the lower troposphere. Corresponding to the composite time series of precipitation, in Fig. 2, the peak intensity for the weak rain is ~0.3 mm h^{-1} for WP and ~0.2 mm h^{-1} for EP (Fig. 2), so the former is only 1.5 times as high as the latter.

On the other hand, deep convective precipitation for the weak rain reaches a peak of 0.13 mm h^{-1} for WP while no more than 0.04 mm h^{-1} for EP (Fig. 3). In contrast, shallow precipitation for the weak rain is comparable between the regions. As such, shallow precipitation makes a disproportionally high contributions to the weak rain over EP compared to WP, accounting for a more bottom-heavy ascent for the EP weak rain than for the WP weak rain (Fig. 4). This result, along with the fact that weak and moderate rains occur relatively frequently in EP compared to WP (Table 2), indicates

that the known shallowness of ω profiles in EP is ascribed to weak rain and partially to moderate rain, while the evolution of vertical velocity for strong rain is more or less as expected for the MCS lifecycle in both WP and EP.

Table 2. The sample numbers of the rain intensity among the regions. From 2001 to 2013 (13 years), the sample numbers of strong, moderate, and weak rain events in ITCZ, WP, and EP.

Region \ rain intensity	Strong rain	Moderate rain	Weak rain
ITCZ	44755	20510	25839
WP	4259	1496	1035
EP	3993	1704	2059

5. Conclusion and discussion

This study investigates the fundamental characteristics of convection across the tropical Pacific throughout the convective lifecycle. To this end, GSMaP precipitation is utilized for identifying the local temporal maxima of surface rain, based on which the composite time series of TRMM precipitation and ERA5 vertical motion are obtained to delineate a statistical picture of the convective lifecycle. Composite time series are then decomposed into the three rain intensity classes of strong rain, moderate rain, and weak rain separately for the two representative domains of WP and EP.

The composite time series of total rainfall reveals that the strong and moderate rains are nearly identical across the regions, but the formation mechanism of weak rain appears to change from WP to EP. A decomposition of total rainfall into shallow, deep convective, and stratiform precipitation types shows that the evolutionary features are shared or unshared, depending on rain intensity, between the regions. For strong and moderate rains, deep convective precipitation peaks first and is followed a few hours later by stratiform precipitation in both WP and EP, implying that the occurrence of each rain type follows the same evolution characteristic of MCSs between WP and EP when strong rain systems are singled out. Conversely, for weak rain, deep convective rain still makes the most significant contribution to WP precipitation, while shallow precipitation predominates in EP. The composite time series of vertical motion confirms the well-known top-heavy structure in WP and the bottom-heavy structure in EP. The tilted structure during the convectively active hours in strong and moderate rain is in line with the expectation for the MCS lifecycle. In weak rain, strong upward motion is confined to the lower layers of EP, which is physically consistent with the dominance of shallow precipitation in this region.

Previous studies showed that convective systems exhibit many significant differences between EP and WP, including a higher proportion of shallow and stratiform precipitation and shallower cloud layers over EP (Berg et al. 2002; Schumacher and Houze 2003; Nesbitt et al. 2006; Yokoyama and Takayabu 2012). In WP, a warm pool leads convection to develop deeply. This aligns with our point that total precipitation in the WP is higher than in the EP, with deep convective precipitation being the dominant contributor to each precipitation intensity in WP. In EP, environmental conditions such as lower SSTs and drier air in the troposphere are less conducive to the development of deep convection compared to the WP. The strong SST gradient drives a shallow layer of convergence, resulting in shallow precipitation (Back and Bretherton 2009a). This can also be observed in Fig. 3, where shallow precipitation is more prevalent in both moderate and weak rainfall in the EP.

Additionally, Back et al. (2017) showed that the geographical areas with a high stratiform fraction, including EP, are not apparently correlated with the areas typical of top-heavy ascent. This seemingly unexpected conclusion may be partly because their precipitation samples are constrained to rain rates higher than 5 mm day^{-1} or about 0.2 mm h^{-1}. This condition is met for our strong rain composite while the threshold is too high for the weak rain even at its peak (Fig. 3). Lowering the 5 mm day^{-1} threshold might result in a higher correlation between the stratiform ratio and top-heaviness.

The findings above provide insight into the regional differences in the development mechanism of tropical convection. Specific factors responsible for the weak rain processes have yet to be singled out in future work.

Acknowledgments

This study was supported by a scholarship from the Japan-Taiwan Exchange Association. The author sincerely appreciates the support of the Japan-Taiwan Exchange Association for international scholars.

Edited by: K. Yasunaga

References

Back, L. E., and C. S. Bretherton, 2006: Geographic variability in the export of moist static energy and vertical motion profiles in the tropical Pacific. *Geophys. Res. Lett.*, **33**, L17810, doi:10.1029/2006GL026672.

Back, L. E., and C. S. Bretherton, 2009a: On the relationship between SST gradients, boundary layer winds, and convergence over the tropical oceans. *J. Climate*, **22**, 4182–4196.

Back, L. E., and C. S. Bretherton, 2009b: A simple model of climatological rainfall and vertical motion patterns over

the tropical oceans. *J. Climate*, **22**, 6477–6497.

Back, L. E., Z. Hansen, and Z. Handlos, 2017: Estimating vertical motion profile top-heaviness: Reanalysis compared to satellite-based observations and stratiform rain fraction. *J. Atmos. Sci.*, **74**, 855–864.

Benedict, J. J., and D. A. Randall, 2007: Observed characteristics of the MJO relative to maximum rainfall. *J. Atmos. Sci.*, **64**, 2332–2354.

Berg, W., C. Kummerow, and C. A. Morales, 2002: Differences between east and west Pacific rainfall systems. *J. Climate*, **15**, 3659–3672.

Frank, W. M., and J. L. McBride, 1989: The vertical distribution of heating in AMEX and GATE cloud clusters. *J. Atmos. Sci.*, **46**, 3464–3478.

Handlos, Z. J., and L. E. Back, 2014: Estimating vertical motion profile shape within tropical weather states over the oceans. *J. Climate*, **27**, 7667–7686.

Hersbach, H., B. Bell, P. Berrisford, S. Hirahara, A. Horányi, J. Muñoz-Sabater, J. Nicolas, C. Peubey, R. Radu, D. Schepers, A. Simmons, C. Soci, S. Abdalla, X. Abellan, G. Balsamo, P. Bechtold, G. Biavati, J. Bidlot, M. Bonavita, G. De Chiara, P. Dahlgren, D. Dee, M. Diamantakis, R. Dragani, J. Flemming, R. Forbes, M. Fuentes, A. Geer, L. Haimberger, S. Healy, R. J. Hogan, E. Hólm, M. Janisková, S. Keeley, P. Laloyaux, P. Lopez, C. Lupu, G. Radnoti, P. de Rosnay, I. Rozum, F. Vamborg, S. Villaume, and J.-N. Thépaut, 2020: The ERA5 global reanalysis. *Quart. J. Roy. Meteor. Soc.*, **146**, 1999–2049.

Houze, R. A. Jr., 1989: Observed structure of mesoscale convective systems and implications for large-scale heating. *Quart. J. Roy. Meteor. Soc.*, **115**, 425–461.

Houze, R. A. Jr., 1997: Stratiform precipitation in regions of convection: A meteorological paradox? *Bull. Amer. Meteor. Soc.*, **78**, 2179–2196.

Huffman, G. J., D. T. Bolvin, D. Braithwaite, K. Hsu, R. Joyce, C. Kidd, E. J. Nelkin, S. Sorooshian, J. Tan, and P. Xie, 2019: Algorithm Theoretical Basis Document (ATBD) version 06. NASA Global Precipitation Measurement (GPM) Integrated Multi-satellitE Retrievals for GPM (IMERG).

Inoue, K., and L. Back, 2015a: Column-integrated moist static energy budget analysis on various time scales during TOGA COARE. *J. Atmos. Sci.*, **72**, 1856–1871.

Johnson, R. H., and X. Lin, 1997: Episodic trade wind regimes over the western Pacific warm pool. *J. Atmos. Sci.*, **54**, 2020–2034.

Johnson, R. H., T. M. Rickenbach, S. A. Rutledge, P. E. Ciesielski, and W. H. Schubert, 1999: Trimodal characteristics of tropical convection. *J. Climate*, **12**, 2397–2418.

Kiladis, G. N., M. C. Wheeler, P. T. Haertel, K. H. Straub, and P. E. Roundy, 2009: Convectively coupled equatorial waves. *Rev. Geophys.*, **47**, RG2003, doi:10.1029/2008RG000266.

Kubota, T., K. Aonashi, T. Ushio, S. Shige, Y. N. Takayabu, M. Kachi, Y. Arai, T. Tashima, T. Masaki, N. Kawamoto, T. Mega, M. K. Yamamoto, A. Hamada, M. Yamaji, G. Liu, and R. Oki, 2020: Global Satellite Mapping of Precipitation (GSMaP) products in the GPM era. *Satellite Precipitation Measurement*. V. Levizzani, C. Kidd, D. B. Kirschbaum, C. D. Kummerow, K. Nakamura, and F. J. Turk Eds., Advances in Global Change Research, **67**, Springer, Cham, 355–373.

Kurowski, M. J., K. Suselj, W. W. Grabowski, and J. Teixeira, 2018: Shallow-to-deep transition of continental moist convection: Cold pools, surface fluxes, and mesoscale organization. *J. Atmos. Sci.*, **75**, 4071–4090.

Lamer, K., P. Kollias, and L. Nuijens, 2015: Observations of the variability of shallow trade wind cumulus cloudiness and mass flux. *J. Geophys. Res. Atmos.*, **120**, 6161–6178.

Lappen, C.-L., and C. Schumacher, 2012: Heating in the tropical atmosphere: What level of detail is critical for accurate MJO simulations in GCMs? *Climate Dyn.*, **39**, 2547–2568.

Lappen, C.-L., and C. Schumacher, 2014: The role of tilted heating in the evolution of the MJO. *J. Geophys. Res. Atmos.*, **119**, 2966–2989, doi:10.1002/2013JD020638.

Lindzen, R. S., and S. Nigam, 1987: On the role of sea surface temperature gradients in forcing low-level winds and convergence in the tropics. *J. Atmos. Sci.*, **44**, 2418–2436.

Mapes, B., S. Tulich, J. Lin, and P. Zuidema, 2006: The mesoscale convection life cycle: Building block or prototype for large-scale tropical waves? *Dyn. Atmos. Oceans*, **42**, 3–29.

Masunaga, H., 2012: A satellite study of the atmospheric forcing and response to moist convection over tropical and subtropical oceans. *J. Atmos. Sci.*, **69**, 150–167.

Masunaga, H., 2013: A satellite study of tropical moist convection and environmental variability: A moisture and thermal budget analysis. *J. Atmos. Sci.*, **70**, 2443–2466.

Masunaga, H., and T. S. L'Ecuyer, 2014: A mechanism of tropical convection inferred from observed variability in the moist static energy budget. *J. Atmos. Sci.*, **71**, 3747–3766.

Nesbitt, S. W., R. Cifelli, and S. A. Rutledge, 2006: Storm morphology and rainfall characteristics of TRMM precipita-

tion features. *Mon. Wea. Rev.*, **134**, 2702–2721.

Numaguti, A., R. Oki, K. Nakamura, K. Tsuboki, N. Misawa, T. Aisai, and Y.-M. Kodama, 1995: 4–5-day-period variation and low-level dry air observed in the equatorial western Pacific during the TOGA-COARE IOP. *J. Meteor. Soc. Japan*, **73**, 267–290.

Powell, S. W., R. A. Houze Jr., and S. R. Brodzik, 2016: Rainfall-type categorization of radar echoes using polar coordinate reflectivity data. *J. Atmos. Oceanic Technol.*, **33**, 523–538.

Schumacher, C., and R. A. Houze Jr., 2003: Stratiform rain in the tropics as seen by the TRMM precipitation radar. *J. Climate*, **16**, 1739–1756.

Schumacher, C., R. A. Houze Jr., and I. Kraucunas, 2004: The tropical dynamical response to latent heating estimates derived from the TRMM precipitation radar. *J. Atmos. Sci.*, **61**, 1341–1358.

Sherwood, S. C., 1999: Convective precursors and predictability in the tropical west Pacific. *Mon. Wea. Rev.*, **127**, 2977–2991.

Shige, S., Y. N. Takayabu, W.-K. Tao, and C.-L. Shie, 2007: Spectral retrieval of latent heating profiles from TRMM PR data. Part II: Algorithm improvement and heating estimates over tropical ocean regions. *J. Appl. Meteor. Climatol.*, **46**, 1098–1124.

Sobel, A. H., S. E. Yuter, C. S. Bretherton, and G. N. Kiladis, 2004: Large-scale meteorology and deep convection during TRMM KWAJEX. *Mon. Wea. Rev.*, **132**, 422–444.

Takayabu, Y. N., K.-M. Lau, and C.-H. Sui, 1996: Observation of a quasi-2-day wave during TOGA COARE. *Mon. Wea. Rev.*, **124**, 1892–1913.

Trenberth, K. E., D. P. Stepaniak, and J. M. Caron, 2000: The global monsoon as seen through the divergent atmospheric circulation. *J. Climate*, **13**, 3969–3993.

Ushiyama, T., S. Satoh, and K. Takeuchi, 1995: Time and spatial variations of mesoscale rainfalls and their relation to the large-scale field in the western tropical Pacific. *J. Meteor. Soc. Japan*, **73**, 379–392.

Vogel, R., L. Nuijens, and B. Stevens, 2020: Influence of deepening and mesoscale organization of shallow convection on stratiform cloudiness in the downstream trades. *Quart. J. Roy. Meteor. Soc.*, **146**, 174–185.

Xu, J., Z. Ma, S. Yan, and J. Peng, 2022: Do ERA5 and ERA5-land precipitation estimates outperform satellite-based precipitation products? A comprehensive comparison between state-of-the-art model-based and satellite-based precipitation products over mainland China. *J. Hydrol.*, **605**, 127353, doi:10.1016/j.jhydrol.2021.127353.

Yokoyama, C., and Y. N. Takayabu, 2012: Relationships between rain characteristics and environment. Part I: TRMM precipitation features and the large-scale environment over the tropical Pacific. *Mon. Wea. Rev.*, **140**, 2831–2840.

Yoneyama, K., and T. Fujitani, 1995: The behavior of dry westerly air associated with convection observed during the TOGA-COARE R/V Natsushima cruise. *J. Meteor. Soc. Japan*, **73**, 291–304.

Zhang, C., M. McGauley, and N. A. Bond, 2004: Shallow meridional circulation in the tropical eastern Pacific. *J. Climate*, **17**, 133–139.

Zhang, Y., and S. A. Klein, 2010: Mechanisms affecting the transition from shallow to deep convection over land: Inferences from observations of the diurnal cycle collected at the ARM Southern Great Plains site. *J. Atmos. Sci.*, **67**, 2943–2959.